

# Polarization and Forward-Backward Asymmetry of $\Lambda$ Baryons in Hadronic $Z^0$ Decays

The OPAL Collaboration

## Abstract

The longitudinal polarization, the transverse polarization, and the forward-backward asymmetry of  $\Lambda$  baryons, have been measured using a sample of 4.34 million hadronic  $Z^0$  decays collected with the OPAL detector at LEP between 1990 and 1995. These results are important as an aid to the understanding of hadronization mechanisms. Significant longitudinal polarization has been observed at intermediate and high momentum. For  $x_E (\equiv 2E_\Lambda/\sqrt{s}) > 0.3$ , the longitudinal polarization has been measured to be  $-32.9 \pm 5.5$  (stat)  $\pm 5.2$  (syst)%. We have observed no transverse polarization. A significant forward-backward asymmetry has been measured and can be described by a JETSET model.

(Submitted to Z. Phys. C)

# The OPAL Collaboration

K. Ackerstaff<sup>8</sup>, G. Alexander<sup>23</sup>, J. Allison<sup>16</sup>, N. Altekamp<sup>5</sup>, K.J. Anderson<sup>9</sup>, S. Anderson<sup>12</sup>, S. Arcelli<sup>2</sup>, S. Asai<sup>24</sup>, D. Axen<sup>29</sup>, G. Azuelos<sup>18,a</sup>, A.H. Ball<sup>17</sup>, E. Barberio<sup>8</sup>, R.J. Barlow<sup>16</sup>, R. Bartoldus<sup>3</sup>, J.R. Batley<sup>5</sup>, S. Baumann<sup>3</sup>, J. Bechtluft<sup>14</sup>, C. Beeston<sup>16</sup>, T. Behnke<sup>8</sup>, A.N. Bell<sup>1</sup>, K.W. Bell<sup>20</sup>, G. Bella<sup>23</sup>, S. Bentvelsen<sup>8</sup>, S. Bethke<sup>14</sup>, O. Biebel<sup>14</sup>, A. Biguzzi<sup>5</sup>, S.D. Bird<sup>16</sup>, V. Blobel<sup>27</sup>, I.J. Bloodworth<sup>1</sup>, J.E. Bloomer<sup>1</sup>, M. Bobinski<sup>10</sup>, P. Bock<sup>11</sup>, D. Bonacorsi<sup>2</sup>, M. Boutemeur<sup>34</sup>, B.T. Bouwens<sup>12</sup>, S. Braibant<sup>12</sup>, L. Brigliadori<sup>2</sup>, R.M. Brown<sup>20</sup>, H.J. Burckhart<sup>8</sup>, C. Burgard<sup>8</sup>, R. Bürgin<sup>10</sup>, P. Capiluppi<sup>2</sup>, R.K. Carnegie<sup>6</sup>, A.A. Carter<sup>13</sup>, J.R. Carter<sup>5</sup>, C.Y. Chang<sup>17</sup>, D.G. Charlton<sup>1,b</sup>, D. Chrisman<sup>4</sup>, P.E.L. Clarke<sup>15</sup>, I. Cohen<sup>23</sup>, J.E. Conboy<sup>15</sup>, O.C. Cooke<sup>8</sup>, M. Cuffiani<sup>2</sup>, S. Dado<sup>22</sup>, C. Dallapiccola<sup>17</sup>, G.M. Dallavalle<sup>2</sup>, R. Davis<sup>30</sup>, S. De Jong<sup>12</sup>, L.A. del Pozo<sup>4</sup>, K. Desch<sup>3</sup>, B. Dienes<sup>33,d</sup>, M.S. Dixit<sup>7</sup>, E. do Couto e Silva<sup>12</sup>, M. Doucet<sup>18</sup>, E. Duchovni<sup>26</sup>, G. Duckeck<sup>34</sup>, I.P. Duerdoth<sup>16</sup>, D. Eatough<sup>16</sup>, J.E.G. Edwards<sup>16</sup>, P.G. Estabrooks<sup>6</sup>, H.G. Evans<sup>9</sup>, M. Evans<sup>13</sup>, F. Fabbri<sup>2</sup>, M. Fanti<sup>2</sup>, A.A. Faust<sup>30</sup>, F. Fiedler<sup>27</sup>, M. Fierro<sup>2</sup>, H.M. Fischer<sup>3</sup>, I. Fleck<sup>8</sup>, R. Folman<sup>26</sup>, D.G. Fong<sup>17</sup>, M. Foucher<sup>17</sup>, A. Fürstjes<sup>8</sup>, D.I. Futyan<sup>16</sup>, P. Gagnon<sup>7</sup>, J.W. Gary<sup>4</sup>, J. Gascon<sup>18</sup>, S.M. Gascon-Shotkin<sup>17</sup>, N.I. Geddes<sup>20</sup>, C. Geich-Gimbel<sup>3</sup>, T. Gerialis<sup>20</sup>, G. Giacomelli<sup>2</sup>, P. Giacomelli<sup>4</sup>, R. Giacomelli<sup>2</sup>, V. Gibson<sup>5</sup>, W.R. Gibson<sup>13</sup>, D.M. Gingrich<sup>30,a</sup>, D. Glenzinski<sup>9</sup>, J. Goldberg<sup>22</sup>, M.J. Goodrick<sup>5</sup>, W. Gorn<sup>4</sup>, C. Grandi<sup>2</sup>, E. Gross<sup>26</sup>, J. Grunhaus<sup>23</sup>, M. Gruwé<sup>8</sup>, C. Hajdu<sup>32</sup>, G.G. Hanson<sup>12</sup>, M. Hansroul<sup>8</sup>, M. Hapke<sup>13</sup>, C.K. Hargrove<sup>7</sup>, P.A. Hart<sup>9</sup>, C. Hartmann<sup>3</sup>, M. Hauschild<sup>8</sup>, C.M. Hawkes<sup>5</sup>, R. Hawkings<sup>27</sup>, R.J. Hemingway<sup>6</sup>, M. Herndon<sup>17</sup>, G. Herten<sup>10</sup>, R.D. Heuer<sup>8</sup>, M.D. Hildreth<sup>8</sup>, J.C. Hill<sup>5</sup>, S.J. Hillier<sup>1</sup>, P.R. Hobson<sup>25</sup>, R.J. Homer<sup>1</sup>, A.K. Honma<sup>28,a</sup>, D. Horváth<sup>32,c</sup>, K.R. Hossain<sup>30</sup>, R. Howard<sup>29</sup>, P. Hüntemeyer<sup>27</sup>, D.E. Hutchcroft<sup>5</sup>, P. Igo-Kemenes<sup>11</sup>, D.C. Imrie<sup>25</sup>, M.R. Ingram<sup>16</sup>, K. Ishii<sup>24</sup>, A. Jawahery<sup>17</sup>, P.W. Jeffreys<sup>20</sup>, H. Jeremie<sup>18</sup>, M. Jimack<sup>1</sup>, A. Joly<sup>18</sup>, C.R. Jones<sup>5</sup>, G. Jones<sup>16</sup>, M. Jones<sup>6</sup>, U. Jost<sup>11</sup>, P. Jovanovic<sup>1</sup>, T.R. Junk<sup>8</sup>, D. Karlen<sup>6</sup>, V. Kartvelishvili<sup>16</sup>, K. Kawagoe<sup>24</sup>, T. Kawamoto<sup>24</sup>, P.I. Kaval<sup>30</sup>, R.K. Keeler<sup>28</sup>, R.G. Kellogg<sup>17</sup>, B.W. Kennedy<sup>20</sup>, J. Kirk<sup>29</sup>, A. Klier<sup>26</sup>, S. Kluth<sup>8</sup>, T. Kobayashi<sup>24</sup>, M. Kobel<sup>10</sup>, D.S. Koetke<sup>6</sup>, T.P. Kokott<sup>3</sup>, M. Kolrep<sup>10</sup>, S. Komamiya<sup>24</sup>, T. Kress<sup>11</sup>, P. Krieger<sup>6</sup>, J. von Krogh<sup>11</sup>, P. Kyberd<sup>13</sup>, G.D. Lafferty<sup>16</sup>, R. Lahmann<sup>17</sup>, W.P. Lai<sup>19</sup>, F. Lamarche<sup>18,f</sup>, D. Lanske<sup>14</sup>, J. Lauber<sup>15</sup>, S.R. Lautenschlager<sup>31</sup>, J.G. Layter<sup>4</sup>, D. Lazic<sup>22</sup>, A.M. Lee<sup>31</sup>, E. Lefebvre<sup>18</sup>, D. Lellouch<sup>26</sup>, J. Letts<sup>12</sup>, L. Levinson<sup>26</sup>, S.L. Lloyd<sup>13</sup>, F.K. Loebinger<sup>16</sup>, G.D. Long<sup>28</sup>, M.J. Losty<sup>7</sup>, J. Ludwig<sup>10</sup>, A. Macchiolo<sup>2</sup>, A. Macpherson<sup>30</sup>, M. Mannelli<sup>8</sup>, S. Marcellini<sup>2</sup>, C. Markus<sup>3</sup>, A.J. Martin<sup>13</sup>, J.P. Martin<sup>18</sup>, G. Martinez<sup>17</sup>, T. Mashimo<sup>24</sup>, P. Mättig<sup>3</sup>, W.J. McDonald<sup>30</sup>, J. McKenna<sup>29</sup>, E.A. Mckigney<sup>15</sup>, T.J. McMahon<sup>1</sup>, R.A. McPherson<sup>8</sup>, F. Meijers<sup>8</sup>, S. Menke<sup>3</sup>, F.S. Merritt<sup>9</sup>, H. Mes<sup>7</sup>, J. Meyer<sup>27</sup>, A. Michelini<sup>2</sup>, G. Mikenberg<sup>26</sup>, D.J. Miller<sup>15</sup>, A. Mincer<sup>22,e</sup>, R. Mir<sup>26</sup>, W. Mohr<sup>10</sup>, A. Montanari<sup>2</sup>, T. Mori<sup>24</sup>, M. Morii<sup>24</sup>, U. Müller<sup>3</sup>, S. Mihara<sup>24</sup>, K. Nagai<sup>26</sup>, I. Nakamura<sup>24</sup>, H.A. Neal<sup>8</sup>, B. Nellen<sup>3</sup>, R. Nisius<sup>8</sup>, S.W. O’Neale<sup>1</sup>, F.G. Oakham<sup>7</sup>, F. Odorici<sup>2</sup>, H.O. Ogren<sup>12</sup>, A. Oh<sup>27</sup>, N.J. Oldershaw<sup>16</sup>, M.J. Oreglia<sup>9</sup>, S. Orito<sup>24</sup>, J. Pálincás<sup>33,d</sup>, G. Pásztor<sup>32</sup>, J.R. Pater<sup>16</sup>, G.N. Patrick<sup>20</sup>, J. Patt<sup>10</sup>, M.J. Pearce<sup>1</sup>, R. Perez-Ochoa<sup>8</sup>, S. Petzold<sup>27</sup>, P. Pfeifenschneider<sup>14</sup>, J.E. Pilcher<sup>9</sup>, J. Pinfold<sup>30</sup>, D.E. Plane<sup>8</sup>, P. Poffenberger<sup>28</sup>, B. Poli<sup>2</sup>, A. Posthaus<sup>3</sup>, D.L. Rees<sup>1</sup>, D. Rigby<sup>1</sup>, S. Robertson<sup>28</sup>, S.A. Robins<sup>22</sup>, N. Rodning<sup>30</sup>, J.M. Roney<sup>28</sup>, A. Rooke<sup>15</sup>, E. Ros<sup>8</sup>, A.M. Rossi<sup>2</sup>, P. Routenburg<sup>30</sup>, Y. Rozen<sup>22</sup>, K. Runge<sup>10</sup>, O. Runolfsson<sup>8</sup>, U. Ruppel<sup>14</sup>, D.R. Rust<sup>12</sup>, R. Rylko<sup>25</sup>, K. Sachs<sup>10</sup>, T. Saeki<sup>24</sup>, E.K.G. Sarkisyan<sup>23</sup>, C. Sbarra<sup>29</sup>, A.D. Schaile<sup>34</sup>, O. Schaile<sup>34</sup>, F. Scharf<sup>3</sup>, P. Scharff-Hansen<sup>8</sup>, P. Schenk<sup>34</sup>, J. Schieck<sup>11</sup>, P. Schleper<sup>11</sup>, B. Schmitt<sup>8</sup>, S. Schmitt<sup>11</sup>, A. Schönning<sup>8</sup>, M. Schröder<sup>8</sup>, H.C. Schultz-Coulon<sup>10</sup>, M. Schumacher<sup>3</sup>, C. Schwick<sup>8</sup>, W.G. Scott<sup>20</sup>, T.G. Shears<sup>16</sup>, B.C. Shen<sup>4</sup>, C.H. Shepherd-Themistocleous<sup>8</sup>,

P. Sherwood<sup>15</sup>, G.P. Siroli<sup>2</sup>, A. Sittler<sup>27</sup>, A. Skillman<sup>15</sup>, A. Skuja<sup>17</sup>, A.M. Smith<sup>8</sup>, G.A. Snow<sup>17</sup>, R. Sobie<sup>28</sup>, S. Söldner-Rembold<sup>10</sup>, R.W. Springer<sup>30</sup>, M. Sproston<sup>20</sup>, K. Stephens<sup>16</sup>, J. Steuerer<sup>27</sup>, B. Stockhausen<sup>3</sup>, K. Stoll<sup>10</sup>, D. Strom<sup>19</sup>, P. Szymanski<sup>20</sup>, R. Tafirout<sup>18</sup>, S.D. Talbot<sup>1</sup>, S. Tanaka<sup>24</sup>, P. Taras<sup>18</sup>, S. Tarem<sup>22</sup>, R. Teuscher<sup>8</sup>, M. Thiergen<sup>10</sup>, M.A. Thomson<sup>8</sup>, E. von Törne<sup>3</sup>, S. Towers<sup>6</sup>, I. Trigger<sup>18</sup>, Z. Trócsányi<sup>33</sup>, E. Tsur<sup>23</sup>, A.S. Turcot<sup>9</sup>, M.F. Turner-Watson<sup>8</sup>, P. Utzat<sup>11</sup>, R. Van Kooten<sup>12</sup>, D. VanDenPlas<sup>18,g</sup>, M. Verzocchi<sup>10</sup>, P. Vikas<sup>18</sup>, E.H. Vokurka<sup>16</sup>, H. Voss<sup>3</sup>, F. Wäckerle<sup>10</sup>, A. Wagner<sup>27</sup>, C.P. Ward<sup>5</sup>, D.R. Ward<sup>5</sup>, P.M. Watkins<sup>1</sup>, A.T. Watson<sup>1</sup>, N.K. Watson<sup>1</sup>, P.S. Wells<sup>8</sup>, N. Wermes<sup>3</sup>, J.S. White<sup>28</sup>, B. Wilkens<sup>10</sup>, G.W. Wilson<sup>27</sup>, J.A. Wilson<sup>1</sup>, G. Wolf<sup>26</sup>, T.R. Wyatt<sup>16</sup>, S. Yamashita<sup>24</sup>, G. Yekutieli<sup>26</sup>, V. Zacek<sup>18</sup>, D. Zer-Zion<sup>8</sup>

<sup>1</sup>School of Physics and Space Research, University of Birmingham, Birmingham B15 2TT, UK

<sup>2</sup>Dipartimento di Fisica dell' Università di Bologna and INFN, I-40126 Bologna, Italy

<sup>3</sup>Physikalisches Institut, Universität Bonn, D-53115 Bonn, Germany

<sup>4</sup>Department of Physics, University of California, Riverside CA 92521, USA

<sup>5</sup>Cavendish Laboratory, Cambridge CB3 0HE, UK

<sup>6</sup>Ottawa-Carleton Institute for Physics, Department of Physics, Carleton University, Ottawa, Ontario K1S 5B6, Canada

<sup>7</sup>Centre for Research in Particle Physics, Carleton University, Ottawa, Ontario K1S 5B6, Canada

<sup>8</sup>CERN, European Organisation for Particle Physics, CH-1211 Geneva 23, Switzerland

<sup>9</sup>Enrico Fermi Institute and Department of Physics, University of Chicago, Chicago IL 60637, USA

<sup>10</sup>Fakultät für Physik, Albert Ludwigs Universität, D-79104 Freiburg, Germany

<sup>11</sup>Physikalisches Institut, Universität Heidelberg, D-69120 Heidelberg, Germany

<sup>12</sup>Indiana University, Department of Physics, Swain Hall West 117, Bloomington IN 47405, USA

<sup>13</sup>Queen Mary and Westfield College, University of London, London E1 4NS, UK

<sup>14</sup>Technische Hochschule Aachen, III Physikalisches Institut, Sommerfeldstrasse 26-28, D-52056 Aachen, Germany

<sup>15</sup>University College London, London WC1E 6BT, UK

<sup>16</sup>Department of Physics, Schuster Laboratory, The University, Manchester M13 9PL, UK

<sup>17</sup>Department of Physics, University of Maryland, College Park, MD 20742, USA

<sup>18</sup>Laboratoire de Physique Nucléaire, Université de Montréal, Montréal, Quebec H3C 3J7, Canada

<sup>19</sup>University of Oregon, Department of Physics, Eugene OR 97403, USA

<sup>20</sup>Rutherford Appleton Laboratory, Chilton, Didcot, Oxfordshire OX11 0QX, UK

<sup>22</sup>Department of Physics, Technion-Israel Institute of Technology, Haifa 32000, Israel

<sup>23</sup>Department of Physics and Astronomy, Tel Aviv University, Tel Aviv 69978, Israel

<sup>24</sup>International Centre for Elementary Particle Physics and Department of Physics, University of Tokyo, Tokyo 113, and Kobe University, Kobe 657, Japan

<sup>25</sup>Brunel University, Uxbridge, Middlesex UB8 3PH, UK

<sup>26</sup>Particle Physics Department, Weizmann Institute of Science, Rehovot 76100, Israel

<sup>27</sup>Universität Hamburg/DESY, II Institut für Experimental Physik, Notkestrasse 85, D-22607 Hamburg, Germany

<sup>28</sup>University of Victoria, Department of Physics, P O Box 3055, Victoria BC V8W 3P6, Canada

<sup>29</sup>University of British Columbia, Department of Physics, Vancouver BC V6T 1Z1, Canada

<sup>30</sup>University of Alberta, Department of Physics, Edmonton AB T6G 2J1, Canada

<sup>31</sup>Duke University, Dept of Physics, Durham, NC 27708-0305, USA

<sup>32</sup>Research Institute for Particle and Nuclear Physics, H-1525 Budapest, P O Box 49, Hungary

<sup>33</sup>Institute of Nuclear Research, H-4001 Debrecen, P O Box 51, Hungary

<sup>34</sup>Ludwigs-Maximilians-Universität München, Sektion Physik, Am Coulombwall 1, D-85748 Garching, Germany

<sup>a</sup> and at TRIUMF, Vancouver, Canada V6T 2A3

<sup>b</sup> and Royal Society University Research Fellow

<sup>c</sup> and Institute of Nuclear Research, Debrecen, Hungary

<sup>d</sup> and Department of Experimental Physics, Lajos Kossuth University, Debrecen, Hungary

<sup>e</sup> and Department of Physics, New York University, NY 1003, USA

<sup>f</sup> Now at LeCroy Corp., Chestnut Ridge, NY USA 10977-6499

<sup>g</sup> Now at GEMS-Europe, 78533 Buc CEDEX, France

# 1 Introduction

It is well known that the weak interactions are parity violating. Consequently, fermions produced in  $Z^0$  decays have a longitudinal polarization that depends on their left and right electroweak couplings. The polarization is large for quarks but not directly measurable. Assuming the electroweak Standard Model to hold, the extent to which this longitudinal polarization is transferred to the observed hadrons is an interesting test of hadronization. Moreover, in the absence of beam polarization, the quarks have no transverse polarization component and any observed transverse polarization can only arise during the hadronization phase.

In the case of unpolarized beams, standard electroweak theory predicts for the charge  $-\frac{1}{3}$  quarks from  $Z^0$  decay a longitudinal polarization of  $-0.94$  [1]. The corresponding antiquarks have the same degree of polarization, but with opposite helicity. The polarization varies by  $\pm 2\%$  with the centre-of-mass production polar angle  $\theta$ . Gluon radiation will reduce this value slightly – a one-loop QCD calculation [2] shows that this reduction is about  $3\%$ . Therefore, we expect that strange quarks from  $Z^0$  decays will have a polarization of  $-91\%$ , with an uncertainty of a few percent.

The possibility to measure the quark helicities from the polarization of the leading baryons was first suggested in [3]. In the simple quark model the  $\Lambda^1$  spin is given by the spin of the constituent s quark, and the polarization of the primary s quark will be transferred to a directly produced leading  $\Lambda$ . According to the JETSET Monte Carlo program [4] a fraction of  $\Lambda$  will contain the primary s quark from  $e^+e^- \rightarrow Z^0 \rightarrow s\bar{s}$ , in particular those with high momentum. It is these  $\Lambda$ , through a study of their weak decays, that are thus expected to reveal the most information about the polarization of the initial s quark. In addition, during decays of heavier baryon resonances containing the original quark some of the initial quark polarization is expected to be transferred to the final  $\Lambda$ .

Parity violation in the weak decay of  $\Lambda \rightarrow p\pi$  leads to an angular distribution of the decay proton given by

$$\frac{1}{N} \frac{dN}{d \cos \theta^*} = 1 + \alpha P_L \cos \theta^* \quad (1)$$

where  $\cos \theta^*$  is the angle between the proton and the decaying  $\Lambda$  flight directions, transformed to the  $\Lambda$  rest frame, and  $\alpha = 0.642 \pm 0.013$  is the  $\Lambda$  decay parameter [5]. The longitudinal polarization,  $P_L$ , of the  $\Lambda$  can therefore be determined from the distribution of  $\cos \theta^*$ . The dependence of  $P_L$  on  $\Lambda$  momentum is investigated by determining the polarization in a number of  $x_E$  intervals, where the fractional energy of the  $\Lambda$ ,  $x_E$ , is given by  $2E_\Lambda/\sqrt{s}$ .

Several groups have reported that the  $\Lambda$ , as well as other hyperons, produced in fixed-target hadroproduction experiments exhibit significant transverse polarization [6]. However, there is no generally accepted mechanism that can explain the pattern of observed polarizations. It has been suggested [7] that a measurement of the transverse polarization of  $\Lambda$  in  $e^+e^-$  annihilation events could indicate the extent to which final-state interactions contribute to the transverse polarization seen in fixed-target experiments.

The Standard Model of electroweak interactions predicts a forward-backward asymmetry of the fermions produced in  $e^+e^-$  collisions. Pairs of fermions are produced preferentially with the

---

<sup>1</sup>Unless otherwise specified the use of a particle name refers to the particle plus the corresponding antiparticle.

fermion forward and the antifermion backward with respect to the direction of the incoming electron beam. We would expect that those  $\Lambda$  which contain the primary  $s$  quark would reflect this asymmetry, although again there will be a reduction due to fragmentation effects [8].

This paper is organized as follows. The OPAL detector and event samples are described in Section 2. In Section 3 the selection criteria for  $\Lambda$  baryons are given, along with the method of determining the signal and background. The measurement of the longitudinal polarization and associated systematic error are detailed in Sections 4 and 5. In Section 6 we use the JETSET Monte Carlo to predict the longitudinal polarization that we may expect to observe. Section 7 presents the measurement of the transverse polarization and Section 8 the measurement of the  $\Lambda$  forward-backward asymmetry.

## 2 The OPAL Detector and Data Selection

OPAL is a multipurpose detector covering almost the entire solid angle around one of four interaction regions at LEP. Details concerning the detector and its performance are given elsewhere [9]. This analysis relies mainly on the information from the central tracking chambers which are described briefly in this section.

Tracking of charged particles is performed by a central drift chamber system, consisting of a vertex chamber, a jet chamber and  $z$ -chambers<sup>2</sup>. The central detector is positioned inside a solenoid, which provides a uniform magnetic field of 0.435 T. The vertex chamber is a precision drift chamber which covers the range  $|\cos\theta| < 0.95$ . The jet chamber is a large volume drift chamber 4 m long and 3.7 m in diameter which provides tracking in the  $r - \phi$  plane using up to 159 measured space points and in  $z$  by charge division along the wires. The jet chamber also allows the measurement of the specific energy loss of charged particles,  $dE/dx$ . A  $dE/dx$  resolution of 3.5% [10] has been obtained for tracks with  $|\cos\theta| < 0.7$ , allowing particle identification over a large momentum range. A precise measurement of the  $z$ -coordinate is provided by the  $z$ -chambers which surround the jet chamber and cover the range  $|\cos\theta| < 0.72$ . The combination of these chambers leads to a momentum resolution of  $\sigma_{p_t}/p_t \approx \sqrt{0.02^2 + (0.0015 \cdot p_t)^2}$ ,  $p_t$  being the transverse track momentum with respect to the beam direction in GeV, and where the first term represents the contribution from multiple Coulomb scattering.

This analysis is based on the complete data sample collected between 1990 and 1995 with centre-of-mass energies on or near the  $Z^0$  peak. At these energies the longitudinal polarization of the fermions produced in the  $Z^0$  decay is effectively independent of the centre-of-mass energy. With the requirement that all of the central tracking chambers be operational, a total of 4.34 million hadronic  $Z^0$  decays were selected using the criteria described in [11] with an efficiency of  $98.4 \pm 0.4\%$ . The remaining background processes, such as  $e^+e^- \rightarrow \tau^+\tau^-$  and two-photon events, were estimated to be at a negligible level (0.1% or less). Events where the thrust axis lay close to the beam axis were rejected by requiring  $|\cos\theta_{\text{thrust}}| < 0.9$ , where  $\theta_{\text{thrust}}$  is the polar angle of the thrust vector determined from charged tracks. All selected events were used in the determination of the polarization while only events recorded at the  $Z^0$  peak (86% of the data) were used in the measurement of the forward-backward asymmetry as it is expected to vary rapidly with the centre-of-mass energy.

---

<sup>2</sup>In OPAL the coordinate system is defined such that the positive  $z$ -axis is along the direction of the electron beam,  $r$  is the coordinate normal to the beam axis, and  $\theta$  and  $\phi$  are the polar and azimuthal angles.

To determine the selection efficiencies for the  $\Lambda$  baryon, we have used a sample of approximately 3 million JETSET 7.3 and 4 million JETSET 7.4 hadronic  $Z^0$  decays that were processed through the full OPAL detector simulation program [12]. The versions of JETSET have been tuned to agree with overall event shapes and various single particle inclusive distributions and rates as measured by OPAL. Details of the parameters can be found in [13]. The two versions differ mainly in the tuning of the fragmentation parameters and the decay branching ratios of heavy flavour hadrons. The results obtained using the two JETSET samples separately were consistent, so the final results are based on the total combined Monte Carlo sample.

### 3 Selection of $\Lambda$ Candidates and Background Determination

The following procedure is used to select  $\Lambda \rightarrow p\pi$  candidates. All pairs of oppositely charged tracks were checked for intersections in the  $xy$  plane and required to pass the following set of conditions:

- each track must have a transverse momentum,  $p_t$ , in the  $xy$  plane of at least 150 MeV;
- the intersection radius in the  $xy$  plane must lie between 1 and 150 cm from the primary event vertex;
- $\Sigma|d_0|$ , the sum of the absolute values of  $d_0$  ( $d_0$  is defined as the distance of closest approach to the primary event vertex in the  $xy$  plane) for each track, must be larger than 0.2 cm;
- each track must have at least 40 jet chamber hits, and at least 4  $z$ -chamber hits in the barrel region ( $|\cos\theta| < 0.72$ ), or a measurement of the track endpoint in the endcap region of the jet chamber. The cut on the number of jet chamber hits restricts the acceptance to  $|\cos\theta| < 0.93$ ).
- $(\widehat{\vec{r}}, \widehat{\vec{p}})$ , the angle between the vector from the primary vertex to the intersection point and the summed momenta of the tracks, must be less than  $0.5^\circ$  ( $\simeq 8.7$  mrad);
- neither track can have hits more than 2 cm away from the intersection point of the two tracks in the direction of the primary vertex;
- the decay angle of the higher momentum particle (assumed to be a proton),  $|\cos\theta^*|$ , must be less than 0.95. According to the Monte Carlo this requirement reduces the  $\gamma \rightarrow e^+e^-$  conversion background to levels that are below 1% of the total sample for  $x_E$  between 0.05 and 0.09 and to an insignificant amount above  $x_E = 0.3$ . Any remaining  $\gamma$  conversion events are therefore neglected in the following analysis.
- if the higher momentum track has more than 20 hits contributing to the  $dE/dx$  measurement, the probability<sup>3</sup> of the track being a proton is required to be more than 5%.

---

<sup>3</sup>The  $\chi^2$  probability is calculated from the difference between the measured and expected  $dE/dx$  for a given particle type, in units of the  $dE/dx$  resolution, assuming a Gaussian distribution.

All track pairs passing these cuts are then refitted. Both tracks are constrained to originate from a common vertex in  $z$  to improve the invariant mass resolution. The total  $\chi^2$  of this fit is required to be acceptable (less than 50). For all track pairs passing this cut the higher momentum track is assumed to be the proton. Track pairs with a summed momentum of at least 500 MeV ( $x_E = 0.027$ ) are accepted for further analysis. The invariant mass of the pair,  $M_{p\pi}$ , and the decay angle,  $\cos\theta^*$ , are calculated. The distribution of the invariant mass versus the decay angle, after all of the above selection cuts, is shown in Figure 1a for part of the data sample. The  $\Lambda$  signal can be clearly seen, along with a  $K_s^0$  signal. Shown in Figure 1b is the projection onto the  $M_{p\pi}$  axis for the complete data sample, compared to the Monte Carlo.

The resolution of the  $\Lambda$  mass, in both the data and Monte Carlo samples, was  $2.3 \pm 0.1$  MeV for  $x_E < 0.05$  and  $3.5 \pm 0.2$  MeV for  $0.3 < x_E < 0.4$ . No correction was applied to account for the difference between the magnetic field value used in the Monte Carlo and the value measured in the detector. For this reason there is a slight shift in mass visible in Figure 1b which has no effect in any of the following analyses. The selection efficiency for  $\Lambda \rightarrow p\pi$  decays was 25% at  $x_E = 0.15$ , decreasing to 10% at  $x_E = 0.4$ . These efficiencies are compatible with those given in our most recent paper on strange baryon production [14] in which different  $\Lambda$  selection criteria were used.

The data from  $0.027 \leq x_E \leq 1.0$  were divided into nine  $x_E$  intervals. After the cut on  $\cos\theta^*$  to remove the  $\gamma \rightarrow e^+e^-$  background, 19 bins of equal width between  $-0.95 < \cos\theta^* < 0.95$  were used in each interval. For each bin the number of  $\Lambda$  candidates was determined according to the procedure outlined in the remainder of this section.

Small, yet significant differences have been observed between the momentum spectra seen in the data and those given by the JETSET Monte Carlo for  $\Lambda$  baryons, and to a lesser extent for  $K_s^0$  mesons. The Monte Carlo  $\Lambda$  momentum distribution was weighted by an  $x_E$  dependent factor in order to reproduce the distribution observed in the data [14]. These weights varied from 0.99 at  $x_E = 0.05$  to 0.88 at  $x_E = 0.4$ . Similarly, the  $K_s^0$  momentum distribution from the Monte Carlo was scaled by the ratio of the generated and observed momentum distributions [15]. These weights varied from 1.01 to 1.05.

Along with the  $\Lambda$  signal there are residual backgrounds from two sources: random combinations of oppositely charged pairs of tracks, and  $K_s^0$  decays. The amount of background from each of these sources inside a window around the  $\Lambda$  mass ( $M_\Lambda = 1.115684$  GeV [5]) was calculated from the Monte Carlo simulation. Different windows were used for  $x_E < 0.1$  and  $x_E > 0.1$ , as shown on Figure 1a. A wider window was used at higher momentum due to the degradation of the mass resolution as the momentum of the  $\Lambda$  increases. Since the mass resolution also degrades as  $|\cos\theta^*|$  increases, the window increases in width as  $|\cos\theta^*|$  increases. Combining these two effects, the signal windows as a function of  $\cos\theta^*$  are given by  $|M_{p\pi} - M_\Lambda| < (0.007 + |\cos\theta^*| \times 0.008 \text{ GeV})$  ( $x_E < 0.1$ ) and  $|M_{p\pi} - M_\Lambda| < (0.009 + |\cos\theta^*| \times 0.006 \text{ GeV})$  ( $x_E > 0.1$ ).

In Table 1 the number of  $\Lambda$  extracted in each  $\cos\theta^*$  bin is given, along with the Monte Carlo efficiency and the fractions of  $K_s^0$  and random background, for  $x_E > 0.3$ . The total number of  $\Lambda$  candidates and the calculated background fractions for each  $x_E$  interval are given in Table 2. The number of  $\Lambda$  found in each bin are further corrected by the efficiency to obtain the distribution of the number of  $\Lambda$  that were originally produced in the full data sample, as a function of  $\cos\theta^*$ . From these distributions the longitudinal polarization as a function of  $x_E$  was then determined.



$\cos \theta^*$	Efficiency	Random Background Fraction	$K_s^0$ Fraction	$\Lambda$ Signal
-0.95 - -0.85	0.043	0.421	0.005	197 $\pm$ 31
-0.85 - -0.75	0.075	0.246	0.010	342 $\pm$ 26
-0.75 - -0.65	0.084	0.219	0.014	344 $\pm$ 23
-0.65 - -0.55	0.103	0.189	0.019	384 $\pm$ 24
-0.55 - -0.45	0.112	0.191	0.023	408 $\pm$ 26
-0.45 - -0.35	0.122	0.158	0.034	404 $\pm$ 24
-0.35 - -0.25	0.132	0.122	0.056	458 $\pm$ 24
-0.25 - -0.15	0.143	0.141	0.065	430 $\pm$ 25
-0.15 - -0.05	0.140	0.121	0.073	494 $\pm$ 26
-0.05 - 0.05	0.135	0.140	0.097	490 $\pm$ 26
0.05 - 0.15	0.153	0.149	0.144	536 $\pm$ 28
0.15 - 0.25	0.163	0.164	0.135	566 $\pm$ 28
0.25 - 0.35	0.178	0.173	0.130	580 $\pm$ 30
0.35 - 0.45	0.170	0.213	0.141	532 $\pm$ 30
0.45 - 0.55	0.174	0.234	0.110	519 $\pm$ 30
0.55 - 0.65	0.166	0.300	0.101	446 $\pm$ 31
0.65 - 0.75	0.150	0.328	0.092	453 $\pm$ 32
0.75 - 0.85	0.145	0.411	0.086	385 $\pm$ 35
0.85 - 0.95	0.127	0.444	0.071	341 $\pm$ 31

Table 1: The efficiency, random combination background fraction,  $K_s^0$  fraction and the number of  $\Lambda$  candidates extracted from the data sample, as a function of  $\cos \theta^*$ , for  $x_E > 0.3$ . The  $\Lambda$  signal uncertainty includes contributions from both the random background and  $K_s^0$  fraction uncertainties.

## 4 Measurement of the Longitudinal Polarization

To calculate the polarization for each  $x_E$  range, the efficiency-corrected  $\cos \theta^*$  distribution was fitted to a straight line of the form

$$\frac{1}{N} \frac{dN}{d \cos \theta^*} = 1 + \alpha P_L \cos \theta^*, \quad (2)$$

where  $\alpha = 0.642 \pm 0.013$  is the  $\Lambda$  decay parameter [5]. For  $\bar{\Lambda}$ ,  $\alpha = -0.642 \pm 0.013$  by CP invariance. However, since the helicity of the  $\bar{s}$  quark is expected to be opposite that of the  $s$  quark, the same slope is expected for  $\Lambda$  and  $\bar{\Lambda}$ . The polarization is thus calculated directly from the slope of the fitted line.

The measured values of  $P_L$ , as calculated from the fits, are given in Table 2. From these results we observe an indication of longitudinal polarization for  $\Lambda$  with  $x_E > 0.09$  and a significant polarization for those with  $x_E > 0.2$ . The systematic errors are discussed in the following section, and the results are compared to a JETSET Monte Carlo calculation in Section 6. The fits are good in all  $x_E$  intervals. In Figure 2 the fits for 3 separate  $x_E$  regions are shown, along with the fit for  $x_E > 0.3$ , where the  $\chi^2$  is 19.5 for 19 fitted points.

Since the  $\Lambda$  has a non-zero magnetic moment the spin will precess in the magnetic field of the detector. We have estimated that this effect will cause a change in the polarization of

$x_E$	Total $\Lambda$	Random Background Fraction	$K_s^0$ Fraction	$P_L$ (%)
0.027 – 0.05	22280	0.170	0.092	$1.1 \pm 3.8 \pm 3.0$
0.05 – 0.08	42479	0.181	0.091	$-2.5 \pm 2.2 \pm 2.5$
0.08 – 0.09	11542	0.135	0.036	$0.4 \pm 3.9 \pm 2.2$
0.09 – 0.1	10031	0.140	0.029	$-8.9 \pm 4.2 \pm 3.2$
0.1 – 0.15	35101	0.148	0.034	$-5.7 \pm 2.2 \pm 1.3$
0.15 – 0.2	18139	0.187	0.039	$-9.1 \pm 3.2 \pm 3.5$
0.2 – 0.3	15723	0.218	0.049	$-15.4 \pm 3.7 \pm 3.9$
0.3 – 0.4	5569	0.205	0.072	$-19.3 \pm 6.5 \pm 6.5$
0.4 – 1.0	2950	0.222	0.110	$-45.7 \pm 9.8 \pm 7.7$
0.3 – 1.0	8309	0.210	0.084	$-32.9 \pm 5.5 \pm 5.2$

Table 2: The number of  $\Lambda$  candidates extracted from the data sample, the random background fraction,  $K_s^0$  fraction, and the measured longitudinal polarization of  $\Lambda$  from  $Z^0$  decay. The first error quoted for the polarization is statistical, the second systematic.

no more than 1 – 2%, depending on the momentum of the  $\Lambda$  and the polar angle of the flight direction. We have not included any correction for this effect in our results.

## 5 Systematic Error on the Longitudinal Polarization

Several possible sources of systematic error were identified and studied: background determination, the  $\Lambda$  selection cuts, the acceptance window used to determine the number of  $\Lambda$  events, and the factors used to renormalize the Monte Carlo  $K_s^0$  and  $\Lambda$  momentum distributions. Each of these will be discussed below and the values summarized in Tables 3 and 4.

As was mentioned in the previous section, the polarization is expected to be the same for  $\Lambda$  and  $\bar{\Lambda}$ . This was verified explicitly. For  $x_E > 0.3$  the polarization for  $\Lambda$  ( $\bar{\Lambda}$ ) was measured to be  $-33.4 \pm 7.8\%$  ( $-32.3 \pm 7.9\%$ ), where the errors are statistical only. It was also verified that the polarizations of  $\Lambda$  and  $\bar{\Lambda}$  were consistent in all momentum regions.

The fraction of random background in the signal is not constant as a function of  $\cos\theta^*$  and increases as  $|\cos\theta^*| \rightarrow 1$  (see Table 1). If the background is not properly corrected for, especially at larger values of  $|\cos\theta^*|$ , a significant systematic effect could be introduced. To estimate the effect of the background determination the efficiency corrected  $\cos\theta^*$  distributions were fitted over 3 different sub-intervals:  $-0.75 < \cos\theta^* < 0.95$ ,  $-0.75 < \cos\theta^* < 0.65$  and  $-0.95 < \cos\theta^* < 0.65$ . The systematic error was taken to be the RMS deviation of these fitted values from the value obtained when fitting over the full interval.

The selection cuts used to isolate the  $\Lambda$  signal are also a possible source of systematic error. If a particular cut variable is not well modelled by the Monte Carlo too many or too few events will be removed in either the data or Monte Carlo and a possible systematic error introduced. The calculation of the polarization was repeated for several different values of the most important selection cuts (the  $(\vec{r}, \vec{p})$ ,  $\Sigma|d_0|$ ,  $dE/dx$ , and hit radius cuts). The cut on  $(\vec{r}, \vec{p})$  was varied between  $0.25^\circ$  and  $1.0^\circ$  and the  $\Sigma|d_0|$  cut between 0.2 and 0.4 cm. The  $dE/dx$  probability was varied between 0 (no cut applied) and 10%. The cut on the distance of hits

$x_E$	Selection Cut				
	$(\vec{r}, \vec{p})$	$\Sigma d_0 $	Hit Radius	dE/dx	Total
0.027 – 0.05	1.9	0.4	1.1	0.7	2.3
0.05 – 0.08	1.8	0.6	0.6	0.9	2.2
0.08 – 0.09	1.5	0.8	0.3	0.5	1.8
0.09 – 0.1	1.0	0.3	0.7	0.6	1.9
0.1 – 0.15	0.7	0.4	0.5	0.6	1.1
0.15 – 0.2	1.7	0.7	0.5	1.0	2.2
0.2 – 0.3	0.8	1.7	0.4	1.5	2.4
0.3 – 0.4	1.4	2.2	0.9	1.1	3.0
0.4 – 1.0	2.5	3.4	2.0	3.2	5.6
0.3 – 1.0	1.6	2.2	1.0	1.1	3.1

Table 3: Systematic error contributions (in %) to  $P_L$  from the selection cuts. The total contribution is the sum, added in quadrature, of the individual contributions.

away from the intersection point of the two tracks was varied between 1 and 10 cm. For each cut at least 6 different values of the cut were chosen within the ranges specified and the polarization recalculated for each value. The RMS deviation of these values from the value obtained using the cut default was taken to be the systematic error for that particular selection cut. The contributions from each selection cut as a function of  $x_E$  are given in Table 3, where the total systematic error due to the  $\Lambda$  selection procedure is then obtained by adding the contributions from all cuts in quadrature.

The width of the acceptance window around the  $\Lambda$  mass may also affect the calculation of  $P_L$ . If the window is too narrow,  $\Lambda$  that are reconstructed with an invariant mass a significant distance away from the nominal  $\Lambda$  mass will be lost which could introduce a  $\cos\theta^*$  bias. Since the resolution in the data is almost the same as in the Monte Carlo, it is expected that as long as the window is wide enough to include the signal peak the systematic effects will be small. To investigate the effect of the acceptance window, several additional windows were studied, both narrower and wider than the default. As in the two previous cases, the RMS deviation of the values from the default case was taken to be the systematic error.

The method used to adjust the Monte Carlo momentum distributions such that they agreed with those observed experimentally is another possible source of systematic error. Weighting factors were determined as a function of momentum and applied to the Monte Carlo distributions. These factors each had an experimental error associated with them. The factors were varied by  $\pm 1\sigma$  and the polarization recalculated. The difference from the value determined using the nominal correction factor was taken as the systematic error.

The various contributions to the systematic error are compiled in Table 4. The total systematic error is obtained by adding all of the contributions in quadrature.

## 6 Longitudinal Polarization Prediction

We use the model of Gustafson and Häkkinen [1] to calculate the expected polarization from each of several  $\Lambda$  production sources. The JETSET Monte Carlo has been used to determine

$x_E$	Background Determination	Selection Cuts	Acceptance Window	Momentum Distribution	Total
0.027 – 0.05	0.7	2.3	1.8	0.3	3.0
0.05 – 0.08	0.1	2.2	1.2	0.2	2.5
0.08 – 0.09	1.1	1.8	0.4	0.4	2.2
0.09 – 0.1	2.5	1.9	0.5	0.5	3.2
0.1 – 0.15	0.4	1.1	0.4	0.4	1.3
0.15 – 0.2	2.3	2.2	1.2	0.6	3.5
0.2 – 0.3	2.9	2.4	0.7	0.7	3.9
0.3 – 0.4	5.4	3.0	1.7	1.0	6.5
0.4 – 1.0	4.4	5.6	2.7	1.1	7.7
0.3 – 1.0	3.2	3.1	2.3	1.2	5.2

Table 4: Contributions (in %) to the systematic error on  $P_L$ .

the production rates of  $\Lambda$  from each of these sources, and the calculated polarizations are then compared to the measurements.

It is necessary to distinguish between  $\Lambda$  which are produced directly and those which come from decays of heavier resonances. It is also necessary to distinguish between  $\Lambda$  which contain a primary strange quark and those which contain an s quark produced in the fragmentation process. To estimate the polarization in each of these cases, the following assumptions are made [1]:

- In a simple quark model the spin of the  $\Lambda$  is determined by the spin of the s quark. Therefore, a directly produced  $\Lambda$  should be polarized in the same way as the primary s quark.
- Some  $\Lambda$  will be decay products of heavier baryons which contain the primary s quark. These  $\Lambda$  will inherit some fraction of the parent’s polarization. Estimates are given for the  $\Sigma^0$ ,  $\Xi^-$ ,  $\Sigma(1385)^\pm$ , and  $\Xi(1530)$ .
- If a  $\Lambda$  contains a primary u or d quark, that quark becomes part of a spin-0 ud diquark pair, and it is assumed the polarization of the initial quark is lost in the formation of the  $\Lambda$ .
- Quarks produced in the fragmentation process are expected to have no longitudinal polarization and consequently  $\Lambda$  containing these quarks will not be polarized.

It is therefore expected that much of the contribution to an observable polarization will come from  $\Lambda$  that contain the initial s quark, either directly or via a decay. Contributions from the decay of the  $\Omega^-$  can be neglected due to its very low production rate. There will likely be some contribution from the decays of charm and beauty baryons, but just how much of the quark polarization that will be transferred to the  $\Lambda$  is unknown.

It is possible to use the JETSET Monte Carlo to predict the relative abundances of  $\Lambda$  from the various production sources as a function of  $x_E$ . Two versions of JETSET version 7.4 were used. The first version uses the default version of the “popcorn” model for baryon production [16] and has been tuned by OPAL. The parameter set used (see [13]) results

$\Lambda$ Source	$\Lambda$ Polarization	$x_E > 0.15$		$x_E > 0.3$		$x_E > 0.4$	
		Default	MOPS	Default	MOPS	Default	MOPS
Fragmentation	0.	0.461	0.566	0.254	0.398	0.177	0.344
u	0.	0.020	0.028	0.036	0.054	0.044	0.069
d	0.	0.015	0.023	0.027	0.044	0.034	0.056
direct s	-0.91	0.152	0.071	0.278	0.137	0.355	0.175
$\Sigma^0$	-0.10	0.010	0.024	0.018	0.046	0.022	0.059
$\Sigma^*$	-0.51	0.055	0.037	0.096	0.068	0.110	0.077
$\Xi$	-0.55	0.058	0.034	0.103	0.064	0.123	0.074
$\Xi^*$	-0.46	0.008	0.011	0.014	0.020	0.016	0.022
$\Omega^-$	0.	0.001	0.001	0.001	0.002	0.001	0.002
c baryon	-0.25	0.086	0.072	0.112	0.098	0.088	0.083
b baryon	-0.25	0.073	0.063	0.045	0.046	0.025	0.031
b meson	0.	0.061	0.070	0.016	0.023	0.005	0.008
Predicted Polarization (%)		-24.3	-14.5	-40.6	-24.4	-48.4	-28.4

Table 5: Relative contributions to the  $\Lambda$  rate for  $x_E > 0.15$ , 0.3 and 0.4 in the default version of the JETSET popcorn scheme and the modified popcorn scheme (MOPS).

from a global fit to OPAL measurements of event shape distributions, mean charged particle multiplicities, single particle inclusive momentum spectra for  $\pi^\pm$ ,  $K^\pm$ ,  $p(\bar{p})$  and  $\Lambda$  ( $\bar{\Lambda}$ ); and to LEP measurements of the single particle inclusive production rates of 26 hadrons identified in  $Z^0$  decays. Even with this additional tuning significant differences still exist between the predicted and observed rates and momentum spectra of several baryons [14]. Recently however, a modified popcorn scheme has been proposed [17] which incorporates a more complete implementation of baryon production within the LUND string fragmentation model. This version is also used with the OPAL tuning, together with an adjustment of  $\text{PARJ}(10)$ <sup>4</sup> to 2.8, to obtain better agreement with the observed baryon rates and the  $\Lambda$  momentum distribution.

In Table 5 the sources of origin of the  $\Lambda$  are given as predicted by both the default and modified versions of the popcorn scheme for  $x_E > 0.15$ , 0.3 and 0.4. The contribution to the polarization from each source is also given (according to the method of [1], except that we have assumed an additional contribution of 25% for  $\Lambda$  from the decays of charm and bottom flavoured baryons). This assumption is based on a measurement of the  $\Lambda_b$  polarization at LEP [18]. The calculated polarization is shown in Figure 3 for both the default and modified versions of the popcorn scheme. The modified popcorn scheme predicts less polarization, due mostly to the reduced rate of direct  $\Lambda$  production in that model (for example, for  $x_E > 0.3$  only 13.7% of  $\Lambda$  contain the primary s quark directly, compared to 27.8% in the default popcorn version).

The agreement between the predicted longitudinal polarization of the two JETSET versions and the measurements is quite good over the entire momentum range. No clear discrimination between the two versions is possible. There are probably other effects that must be considered beyond the model used here. However, even with these simple assumptions, the observed polarization is reasonably well modelled.

<sup>4</sup>In the modified popcorn scheme there is a suppression of leading baryons. In order to obtain the proper amount of final baryons, a scale factor ( $\text{PARJ}(10)$ ) is applied to  $\text{PARJ}(1)$ , the suppression factor for diquark production.

$p_T$ (GeV/c)	$P_T^\Lambda$ (%)
< 0.3	$-1.8 \pm 3.1 \pm 1.0$
0.3 – 0.6	$0.4 \pm 1.8 \pm 0.7$
0.6 – 0.9	$1.0 \pm 1.9 \pm 0.7$
0.9 – 1.2	$0.8 \pm 2.2 \pm 0.6$
1.2 – 1.5	$0.0 \pm 2.7 \pm 0.6$
> 1.5	$1.8 \pm 1.6 \pm 0.5$
> 0.3	$0.9 \pm 0.9 \pm 0.3$
> 0.6	$1.1 \pm 1.0 \pm 0.4$

Table 6: Measured transverse polarization of  $\Lambda$  baryons as a function of  $p_T$  (the transverse momentum of the  $\Lambda$  measured relative to the event thrust axis). The first error is statistical, the second systematic.

## 7 Measurement of the Transverse Polarization

It has been observed that in hadron-hadron collisions  $\Lambda$  baryons obtain a significant polarization in the direction perpendicular to the event plane. Several models (see [6] and references therein) have been put forward to explain this effect but, as yet, there is no accepted explanation. In  $e^+e^-$  annihilation the transverse polarization of the primary quarks is suppressed by a factor  $m_q/\sqrt{s}$  from helicity conservation, so any transverse polarization will arise only in the hadronization phase [7].

The transverse polarization is investigated along a direction,  $\hat{a} = \hat{p}_\Lambda \times \hat{p}_{\text{thrust}}$ , where  $\hat{p}_\Lambda$  is the  $\Lambda$  direction and  $\hat{p}_{\text{thrust}}$  is the direction of the thrust axis in the  $\Lambda$  hemisphere. The method to determine the transverse polarization is very similar to that used to measure the longitudinal polarization. The function given by Equation (1) is fitted to an efficiency corrected distribution of  $\cos \phi_p$ , where  $\phi_p$  is the angle in the  $\Lambda$  rest frame between the proton and  $\hat{a}$ .

A  $p\pi$  mass selection window of constant width as a function of  $\cos \phi_p$  was used. The width of the window increased with  $x_E$  to account for the worsening of the mass resolution with increasing momentum. For  $x_E < 0.08$  a window of width  $\pm 8$  MeV from the nominal  $\Lambda$  mass was used, for  $0.08 < x_E < 0.1$  the width was  $\pm 11$  MeV, for  $0.1 < x_E < 0.3$  it was  $\pm 15$  MeV and for  $x_E > 0.3$  it was  $\pm 20$  MeV. All other selection cuts were the same as those used in the  $P_L$  analysis, and the method of determining the efficiency-corrected distributions was identical.

The data were binned in  $p_T$ , where  $p_T$  is the transverse momentum of the  $\Lambda$  measured relative to the thrust axis. The results of the fits for several  $p_T$  intervals are shown in Figure 4. As in the longitudinal polarization analysis, the transverse polarization,  $P_T^\Lambda$ , is given by the slope of the fitted line divided by the  $\Lambda$  decay parameter,  $\alpha$ . The results of these fits are given in Table 6. Since the random background in this case has no significant dependence on  $\cos \phi_p$ , it is assumed that there is no systematic effect due to the determination of that background. All other systematic error contributions were determined following the same procedure as was used in the  $P_L$  analysis. Additionally, there were no significant differences found between the values measured for  $\Lambda$  and  $\bar{\Lambda}$ . For example, for  $p_T > 0.3$  GeV/c, the transverse polarization measured for  $\Lambda$  was  $1.9 \pm 1.4\%$  and for  $\bar{\Lambda}$  the value obtained was  $1.5 \pm 1.4\%$  (statistical errors only).

From the results shown in Table 6 we conclude that there is no evidence for any significant

transverse polarization of  $\Lambda$  baryons over the entire range of  $p_T$ . As was mentioned previously, it is expected that the primary quarks will not be transversely polarized. This is investigated by applying an energy cut and studying only those  $\Lambda$  with  $x_E > 0.15$ . The result for the transverse polarization of these  $\Lambda$  is  $P_T^\Lambda = -0.4 \pm 2.3\%$  (statistical error only) for  $p_T > 0.3$  GeV/ $c$ . In addition, we have studied the transverse polarization in and out of the scattering plane. If the thrust axis is replaced by the  $z$ -axis, the transverse polarization out of the scattering plane, along the direction  $\hat{p}_\Lambda \times \hat{z}$ , is found to be  $-1.1 \pm 1.8\%$ . In the scattering plane, along the direction defined by  $\hat{p}_\Lambda \times (\hat{z} \times \hat{p}_\Lambda)$ , the polarization is found to be  $-1.3 \pm 1.7\%$ . The errors are statistical errors only.

## 8 Measurement of the Forward-Backward Asymmetry

The  $\Lambda$  forward-backward asymmetry has also been measured over the same  $x_E$  range as the longitudinal polarization. It is expected that for high momentum  $\Lambda$  this asymmetry will reflect the original  $s$  quark asymmetry [8]. In this part of the analysis the corrected distributions of  $B \cos \theta$  were used to determine  $A_{FB}$ , where  $B$  is the baryon number and  $\theta$  is measured with respect to the direction of the incoming electron beam.

From the efficiency-corrected distributions of  $B \cos \theta$  the forward-backward asymmetry is calculated from:

$$A_{FB} = \frac{N_F - N_B}{N_F + N_B} \quad (3)$$

where  $N_F$  is the total number with  $B \cos \theta > 0$  and  $N_B$  the total number with  $B \cos \theta < 0$ . The values of  $A_{FB}$  calculated with Equation (3) are given in Table 7, as well as the values calculated from the OPAL tuned version of the JETSET Monte Carlo, with and without the modified popcorn scheme. The first error is statistical, the second systematic. The random background was symmetric about  $\cos \theta = 0$  and it was found to give a negligible contribution to the systematic error. The other contributions to the systematic error were determined using the same procedures as those used for the longitudinal polarization analysis. In Figure 5 the measurements are plotted along with curves showing the predictions from both the default OPAL version of JETSET and the modified popcorn version. The agreement between the measurements and the JETSET models is good, but the present statistics do not allow a distinction between models.

## 9 Discussion and Conclusions

We have observed significant values of longitudinal polarization for  $\Lambda$  with intermediate and high momentum. For  $x_E > 0.3$  the polarization has been measured to be

$$-32.9 \pm 7.6\%$$

The total error is given by the statistical and systematic errors added in quadrature. This value is in agreement with that reported by the ALEPH Collaboration [19] who have measured  $P_L = -32 \pm 7\%$  for  $z = p/p_{\text{beam}} (\simeq x_E) > 0.3$ . The longitudinal polarization results are

$x_E$	$A_{FB}$ (measured)	$A_{FB}$ (JETSET default)	$A_{FB}$ (modified popcorn)
0.027 – 0.05	$-0.007 \pm 0.008 \pm 0.006$	0.003	0.003
0.05 – 0.08	$0.005 \pm 0.005 \pm 0.005$	0.005	0.004
0.08 – 0.09	$-0.008 \pm 0.009 \pm 0.005$	0.009	0.006
0.09 – 0.1	$0.022 \pm 0.010 \pm 0.006$	0.010	0.008
0.1 – 0.15	$0.030 \pm 0.005 \pm 0.006$	0.018	0.013
0.15 – 0.2	$0.033 \pm 0.008 \pm 0.006$	0.027	0.022
0.2 – 0.3	$0.029 \pm 0.008 \pm 0.006$	0.040	0.034
0.3 – 0.4	$0.068 \pm 0.015 \pm 0.008$	0.056	0.043
0.4 – 1.0	$0.102 \pm 0.021 \pm 0.008$	0.074	0.058
0.15 - 1.0	$0.047 \pm 0.005 \pm 0.006$	0.045	0.036
0.3 - 1.0	$0.083 \pm 0.012 \pm 0.006$	0.062	0.050

Table 7: Experimentally determined  $A_{FB}$  for  $\Lambda$  baryons. The first error is statistical, the second is systematic.

reasonably well modelled using a simple quark model and the JETSET Monte Carlo, which has been tuned using LEP data. However, as is discussed in [20], the interpretation of the results is not unique. We have also investigated the transverse polarization of  $\Lambda$  baryons. No significant evidence was found for any transverse polarization. This is consistent with the result reported by ALEPH [19].

For  $x_E > 0.15$  the  $\Lambda$  forward-backward asymmetry was found to be

$$0.047 \pm 0.008.$$

This is in agreement with the value of  $0.0450 \pm 0.0053$  reported by ALEPH [19]. At higher momenta,  $x_E > 0.3$ , the asymmetry was measured to be

$$0.083 \pm 0.013,$$

again in agreement with the ALEPH result of  $0.085 \pm 0.012$ , and the DELPHI [21] result of  $0.085 \pm 0.039$  measured in the range  $0.25 < z < 0.5$  ( $z = p/p_{\text{beam}}$ ). The measurements are also in agreement with the expectation from JETSET.

## Acknowledgements

We particularly wish to thank the SL Division for the efficient operation of the LEP accelerator at all energies and for their continuing close cooperation with our experimental group. We thank our colleagues from CEA, DAPNIA/SPP, CE-Saclay for their efforts over the years on the time-of-flight and trigger systems which we continue to use. In addition to the support staff at our own institutions we are pleased to acknowledge the Department of Energy, USA, National Science Foundation, USA, Particle Physics and Astronomy Research Council, UK, Natural Sciences and Engineering Research Council, Canada, Israel Science Foundation, administered by the Israel Academy of Science and Humanities,



Minerva Gesellschaft,  
Benozio Center for High Energy Physics,  
Japanese Ministry of Education, Science and Culture (the Monbusho) and a grant under the  
Monbusho International Science Research Program,  
German Israeli Bi-national Science Foundation (GIF),  
Bundesministerium für Bildung, Wissenschaft, Forschung und Technologie, Germany,  
National Research Council of Canada,  
Hungarian Foundation for Scientific Research, OTKA T-016660, T023793 and OTKA F-023259.

## References

- [1] G. Gustafson and J. Häkkinen, Phys. Lett. **B303** (1993) 350.
- [2] J.G. Körner, A. Pilaftsis and M.M. Tung, Z. Phys. **C63** (1994) 575.
- [3] J.E. Augustin and F.M. Renard, *Proc. LEP Summer Study*, Report CERN 79-01, Vol. 1 (1979) 185;  
J.E. Augustin and F.M. Renard, Nucl. Phys **B162** (1980) 341.
- [4] T. Sjöstrand, Comp. Phys. Comm. **39** (1986) 347;  
T. Sjöstrand and M.Bengtsson, Comp. Phys. Comm. **43** (1987) 367;  
T. Sjöstrand, Comp. Phys. Comm. **82** (1994) 74.
- [5] R.M. Barnett et al., Particle Data Group, Phys. Rev. **D54** (1996) 1.
- [6] A.D. Panagiotou, Int. J. of Mod. Phys. **A5** (1990) 1197.
- [7] W. Lu, Phys. Rev. **D51** (1995) 5305.
- [8] OPAL Collaboration, K. Ackerstaff *et al.*, *Measurement of the Branching Fractions and Forward-Backward Asymmetries of the  $Z^0$  into Light Quarks*, CERN-PPE/97-063, to be published in Z. Phys. C.
- [9] OPAL Collaboration, M. Ahmet *et al.*, Nucl. Instr. and Meth. **A305** (1991) 275.
- [10] M. Hauschild *et al.*, Nucl. Instr. and Meth. **A314** (1992) 74.
- [11] OPAL Collaboration, G. Alexander *et al.*, Z. Phys. **C52** (1991) 175.
- [12] J. Allison *et al.*, Nucl. Instr. and Meth. **A317** (1992) 47.
- [13] OPAL Collaboration, P.D. Acton *et al.*, Z. Phys. **C58** (1993) 387;  
OPAL Collaboration, R. Akers *et al.*, Z. Phys. **C69** (1996) 543.
- [14] OPAL Collaboration, G. Alexander *et al.*, Z. Phys. **C73** (1997) 569.
- [15] OPAL Collaboration, G. Alexander *et al.*, Z. Phys. **C67** (1995) 389.
- [16] B. Andersson *et al.*, Physica Scripta **32** (1985) 574.
- [17] P. Edén and G. Gustafson, Z. Phys. **C75** (1997) 41;  
P. Edén, *A Program For Baryon Generation and Its Applications to Baryon Fragmentation in DIS*, Lund Preprint LU TP 96-29.
- [18] ALEPH Collaboration, D. Buskulic *et al.*, Phys. Lett. **B365** (1996) 437.
- [19] ALEPH Collaboration, D. Buskulic *et al.*, Phys. Lett. **B374** (1996) 319.
- [20] A. Kotzinian, A. Bravar and D. von Harrach,  *$\Lambda$  and  $\bar{\Lambda}$  Polarization in Lepton Induced Processes*, preprint hep-ph 9701384, to be published in Z. Phys. C.
- [21] DELPHI Collaboration, P. Abreu *et al.*, Z. Phys. **C67** (1995) 1.

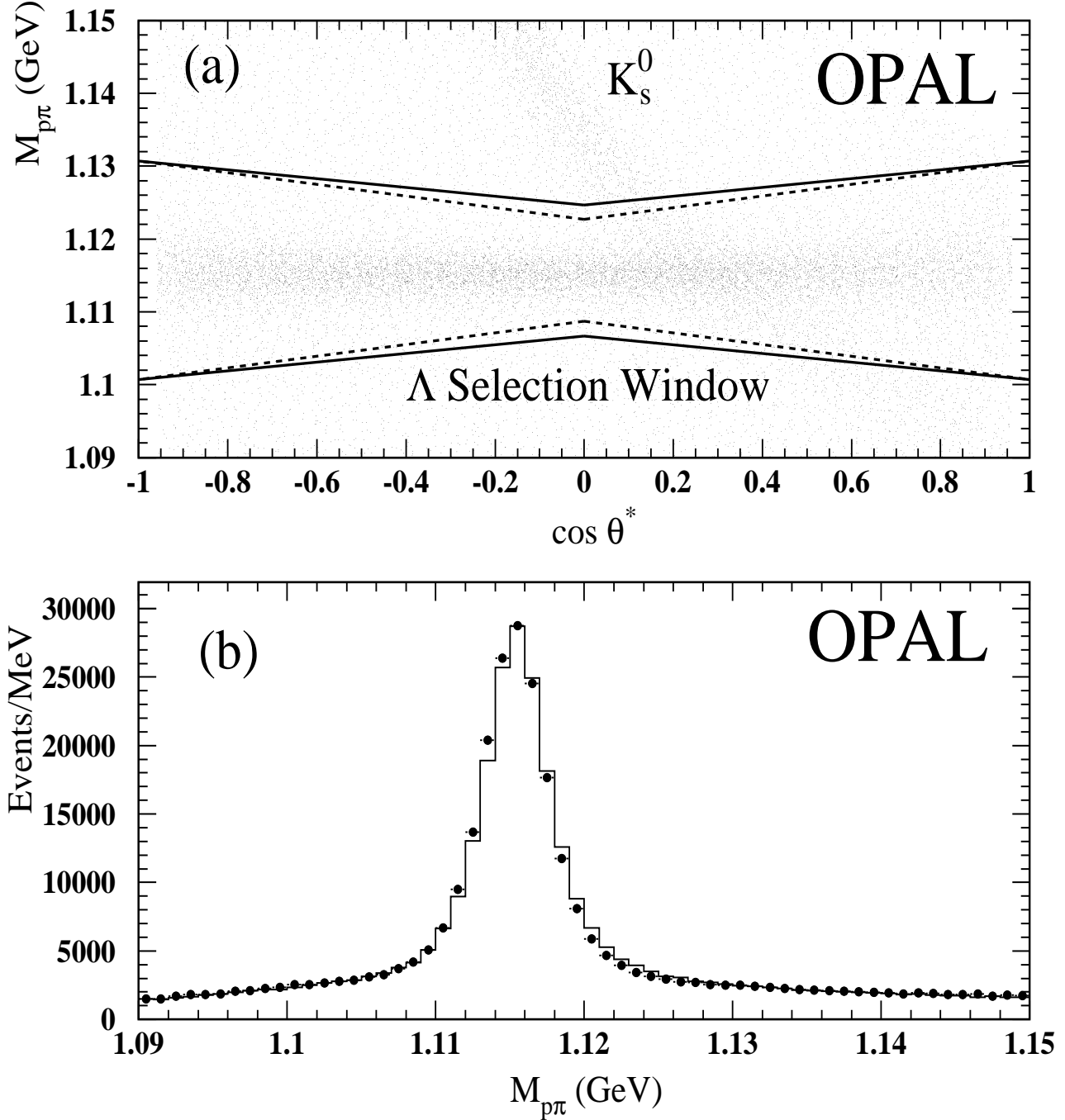


Figure 1: (a) Invariant mass of  $\Lambda$  candidates versus  $\cos \theta^*$  after selection cuts. The window for selecting  $\Lambda$  is shown as a dashed line ( $x_E < 0.1$ ) and a solid line ( $x_E > 0.1$ ). The  $K_s^0 - \Lambda$  overlap region can also be seen around  $\cos \theta^* = 0.2$ . (b) The invariant mass of all  $\Lambda$  candidates after the selection cuts. The histogram is from the Monte Carlo, normalized to the number of OPAL data events (solid points).

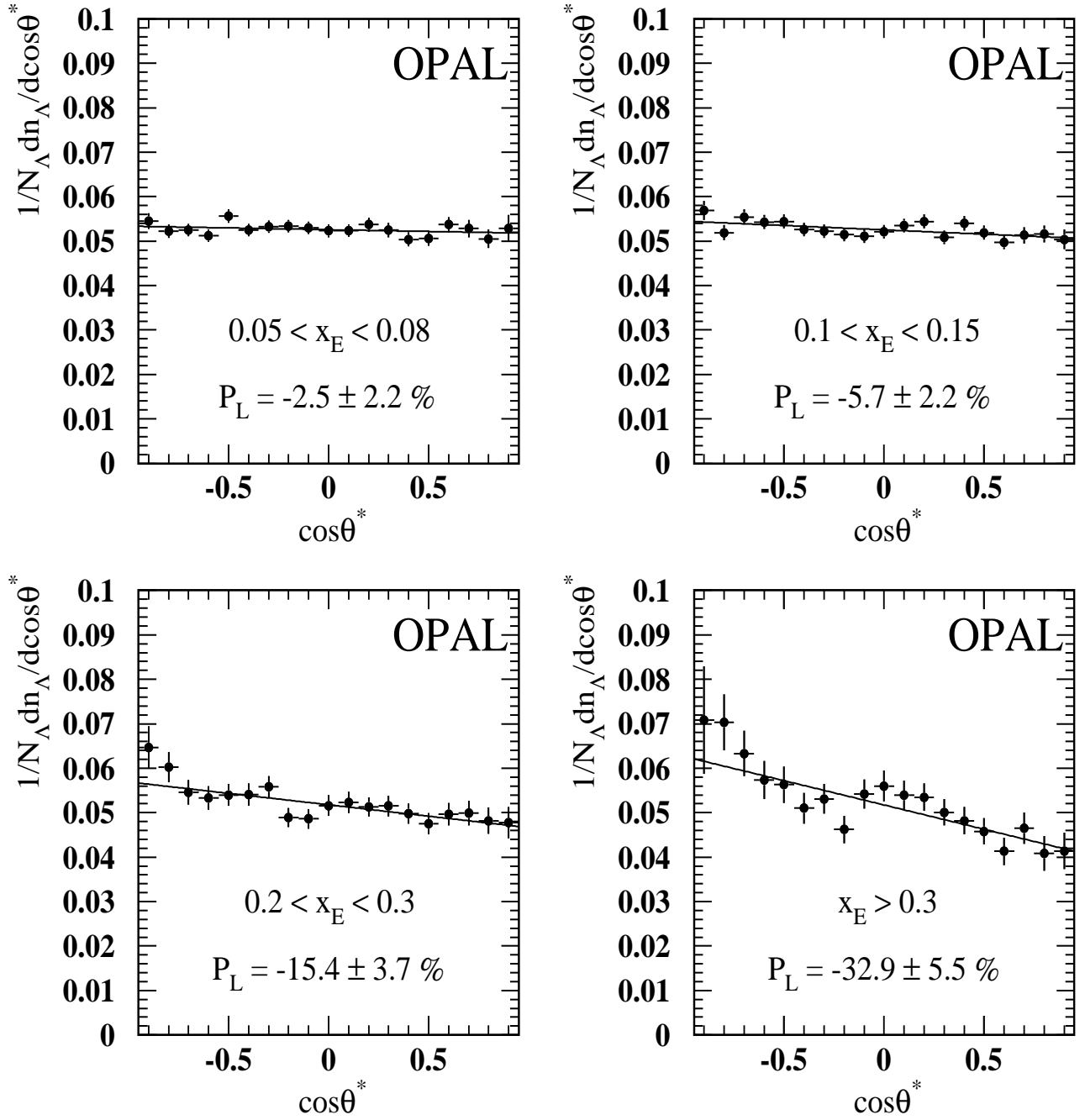


Figure 2: The fits to the efficiency-corrected  $\cos\theta^*$  distributions for several  $x_E$  regions. The error bars are statistical errors only.

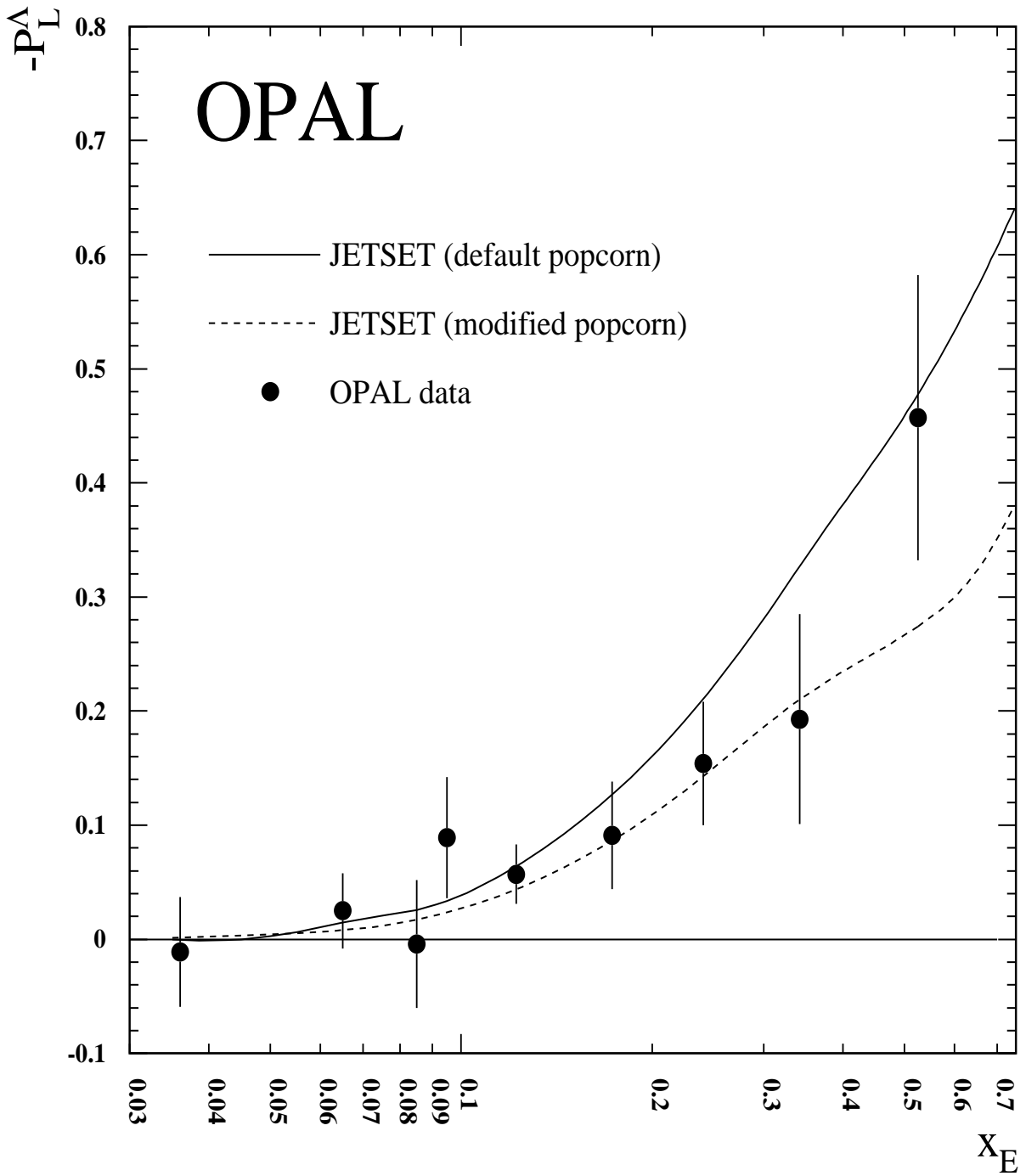


Figure 3: The longitudinal polarization predicted using tuned versions of JETSET with different versions of the popcorn model of baryon production. The measurements are shown as solid points and the error bars are the statistical plus systematic errors, added in quadrature.

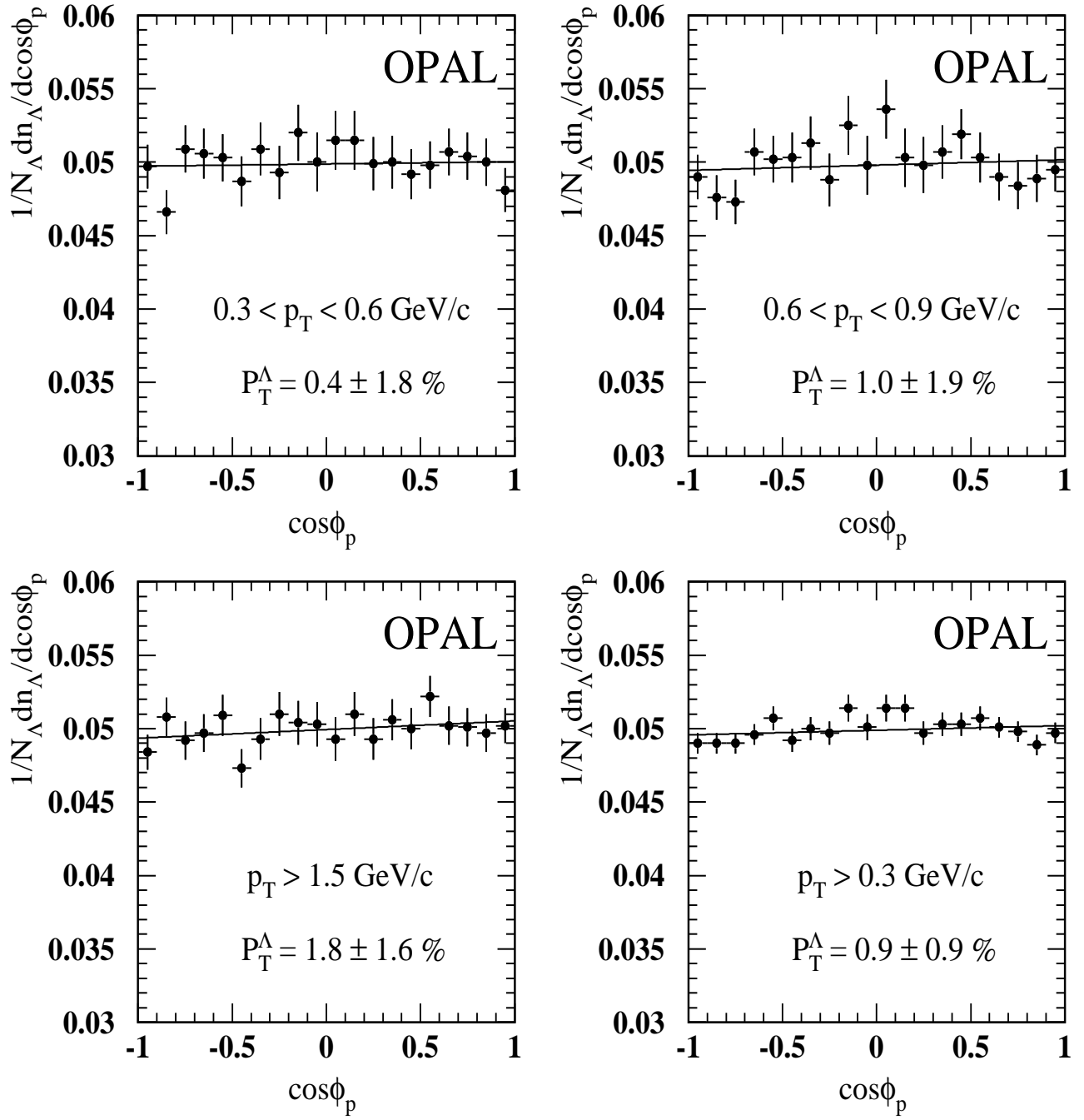


Figure 4: The fits to the efficiency-corrected  $\cos \phi_p$  distributions for several  $p_T$  regions. The error bars are statistical errors only.

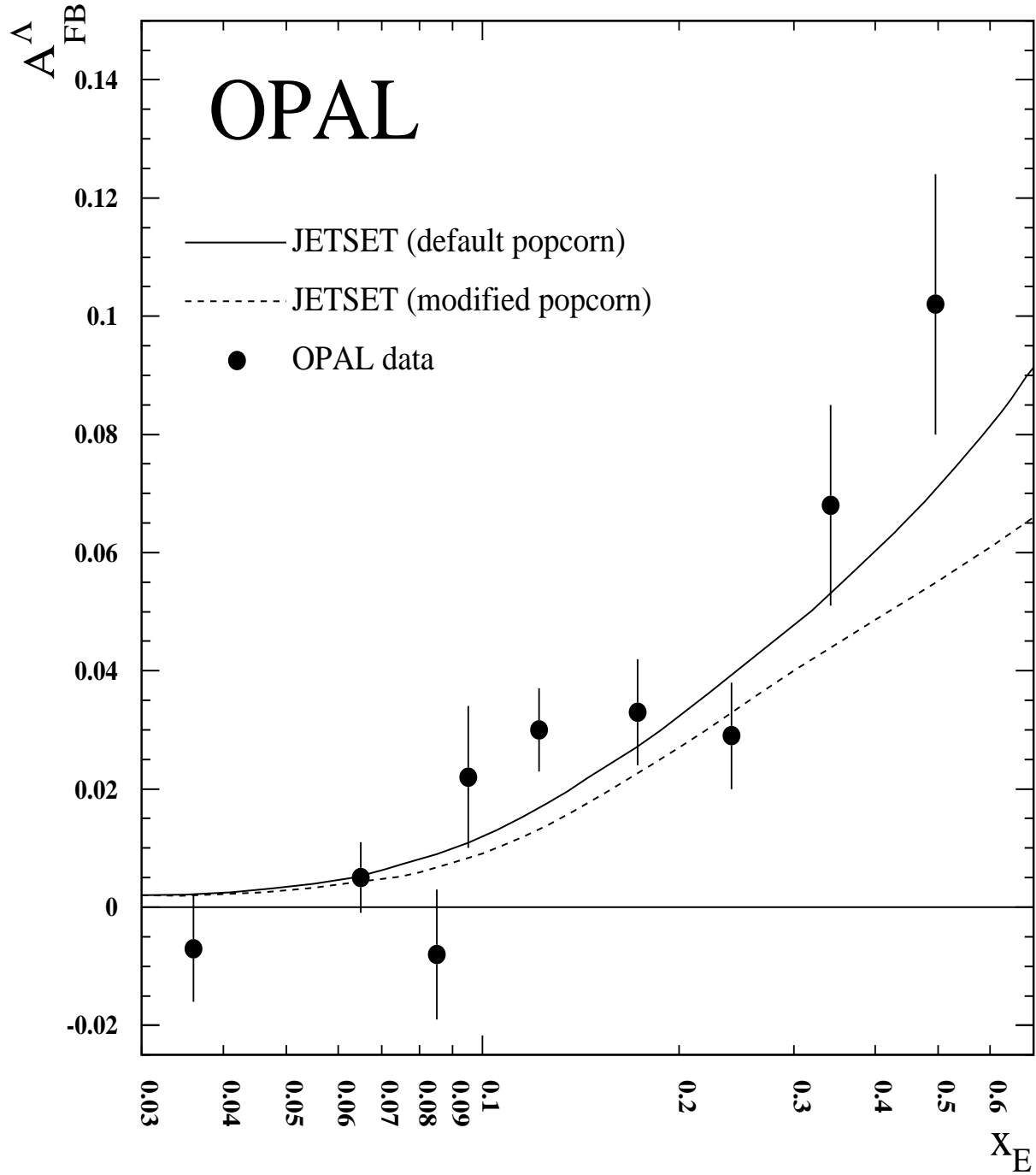


Figure 5: The measured  $\Lambda$  forward-backward asymmetry (solid points) and predictions from JETSET with two different versions of the popcorn model of baryon production. The error bars are statistical and systematic errors, added in quadrature.